GEOPHYSICAL RESEARCH LETTERS, VOL. ???, XXXX, DOI:10.1029/,

Possible evidence for a double crossing phase transition in D″ beneath Central America from inversion of seismic waveforms

Kenji Kawai,[1] Nozomu Takeuchi,[2] Robert J. Geller,[3] and Nobuaki Fuji[3]

We invert seismic body-wave waveform data for the vertical dependence of (isotropic) shear-velocity in the D″ layer beneath Central America, using the transverse components of relatively long period broadband waveforms (20-200 s) as data. Our models suggest that the S-velocity increase in D″ may

---

K. Kawai, Department of Earth and Planetary Sciences, Tokyo Institute of Technology, Ookayama 2-12-1, Meguro-ku, Tokyo, 152-8551, Japan. (kenji@geo.titech.ac.jp)

N. Takeuchi, Earthquake Research Institute, Tokyo University, Yayoi 1-1-1, Bunkyo-ku, Tokyo, 113-0032, Japan. (takeuchi@eri.u-tokyo.ac.jp)

R.J. Geller and N. Fuji, Department of Earth and Planetary Science, Graduate School of Science, Tokyo University, Hongo 7-3-1, Bunkyo-ku, Tokyo, 113-0033, Japan. ([bob,fuji]@eps.s.u-tokyo.ac.jp)

[1]Department of Earth and Planetary Sciences, Tokyo Institute of Technology, Tokyo, Japan.

[2]Earthquake Research Institute, Tokyo University, Tokyo, Japan.

[3]Department of Earth and Planetary Science, Graduate School of Science, Tokyo University, Tokyo, Japan.

be localized in the zone from 100-200 km above the core-mantle boundary (CMB), while the S-velocity does not significantly deviate from PREM in the zone from 0-100 km above the CMB. This suggests the possible existence of a double crossing (a reverse phase transition from post-perovskite back to perovskite) at a depth of 100 km above the CMB. Resolution tests indicate that our methods and data can resolve the vertical velocity profile within D″, and that the lower half of the D″ is especially well resolved.

1. Introduction

The D″ layer, the lowermost 200 km of the mantle, is one of the most important boundary regions in the Earth from the standpoint of geodynamics. Recent experimental studies have found that perovskite (pv), the major component in the lower mantle, makes a phase transition to post-perovskite (ppv) under the pressure-temperature conditions in D″ [*Murakami et al.,* 2004; *Oganov and Ono,* 2004].

Global tomographic studies using travel time data [e.g., *Kennett et al.,* 1998] or long period (e.g., 32 s and longer) waveform inversion [e.g., *Panning and Romanowicz,* 2004] provide gross information on D″, but lack the resolution to reveal its fine structure. 'Local' studies using forward modeling of datasets of body wave waveform data that sample D″ in a particular region have heretofore provided most of our information [*Lay et al.,* 1998; *Wysession et al.,* 1998].

It has been suggested that pv might transform to ppv at the top of D″ but might transform back to pv within D″ because of a strong temperature gradient [*Hernlund et al.,* 2005]. This is called 'double crossing.' With a Clapeyron slope of about 9 MPa/K, a density of 5.6 g/cm^3, and a thickness of D″ of 200 km, the necessary temperature increase is estimated to be 1200 K, which is possible for a thermal boundary of mantle convection [e.g., *Williams,* 1998]. As noted by *Flores and Lay* [2005], it is essentially impossible to determine whether or not 'double crossing' occurs in the Earth by examining individual seismograms. They suggested stacking as one possible approach to the problem [e.g., *Avants et al.,* 2006]. We show below that the simultaneous inversion of a large number of waveforms is also a promising approach.

2. Waveform Inversion

While trial-and-error forward modeling studies have yielded important information, objective and quantitative comparison of synthetics and data is preferable as a method for obtaining information on the structure of the Earth's deep interior. Quantitative inversion procedures allow the use of much larger datasets than is possible in forward modeling studies. Also note that waveform inversion, which considers the variance reduction for the dataset as a whole, is capable of resolving features which are too subtle to generate visually identifiable phases in any single observed seismogram.

Several tools are needed to perform waveform inversion. First, accurate and efficient methods for computing synthetics are required. We have recently developed algorithms based on the Direct Solution Method (DSM) [*Geller and Ohminato,* 1994] for computing highly accurate synthetic seismograms in a spherically symmetric transversely isotropic Earth model [*Kawai et al.,* 2006]. Note that these programs do not use earth-flattening approximations. This software has been released publicly and can be downloaded. At present the publicly released software is only for 1-D media, but this approach can also be applied to 3-D problems [*Takeuchi et al.,* 2000]. Second, the partial derivatives of the synthetics with respect to the model parameters are needed. We use the results of *Geller and Hara* [1993], who formulate the partials for both global (spherical harmonics) and local (pixel) parameterizations. Third, the waveforms that sample D″ pass through the crust, upper mantle, transition zone, and lower mantle, whose effects must be corrected for. As discussed below, we handle this by determining a static correction (time shift) for the observed waveforms before we compare them to the synthetics. Finally, the source

time function (moment rate function) must be known to compute the synthetics. In this study we use earthquakes whose source time duration is sufficiently short to allow the source time function to be approximated as a δ-function at the centroid time for the frequency band used in the data analysis.

Our inverse formulation allows inversion for local ('pixelized') 3-D structure with all 21 elastic coefficients as unknowns. However, due to the limited availability of data and various other uncertainties there are practical limitations on resolution. Because this study is the first attempt at inversion of broadband (up to 20 s period) body-wave waveform data for deep Earth fine structure, we use a laterally homogeneous isotropic model for D″. Note, however, that this is a 1-D model for the target region, rather than a global average.

3. Target region and waveform data

We choose the D″ layer beneath Central America (Fig. 1) as the target region for the inversion. Because of the good distribution of deep sources under South America and of receivers in North America, this region has been extensively studied by previous workers [e.g., *Lay and Helmberger,* 1983; *Kendall and Nangini,* 1996; *Ding and Helmberger,* 1997; *Maupin et al.,* 2005].

We use the transverse components of broadband waveform data (obtained by rotating the N-S and E-W components) for 15 events (Table 1; Fig. 1) from the IRIS/USGS, SCSN, PNSN, BDSN, and CNSN. We apply a bandpass filter to the data and construct datasets for the passband 0.005 to 0.05 Hz (i.e., for the period range, 20-200 s).

We select time windows which include the S and ScS phase from the transverse component records and deconvolve the instrument response. The S and ScS phases are overlapped except for one event (event #12) for which the time windows include only ScS phases. Also, for a few time of these windows diffracted phases are included. We use two selection criteria for data quality. First, we compute the ratio of the maximum amplitude of the data and the corresponding synthetic, and eliminate records for which the ratio is greater than 2 or less than 0.5. Second, records are rejected if the correlation coefficient between the data and synthetics is less than 0.5. The dataset consists of 403 time windows that satisfy the above criteria. 47 records which did not satisfy these criteria were rejected. The reciprocal of the maximum amplitude in each time window is used as the weighting factor in the inversion, so that all data windows have roughly the same importance.

As our dataset consists of relatively long period waveforms, S and ScS phases overlap in more than half of the time windows. Studies based on travel time analysis can treat such waveforms only if the arrival times of each of the overlapping phases can be picked, which is usually not possible. On the other hand, waveform inversion can utilize such phases, which should help to constrain the vertical velocity profile within D″ because overlapped S and ScS at larger distances greater than about 90° (depending on source depth, see Fig. 1) both sample D″ and their behavior gives important information on the velocity structure within D″.

3.1. Time shift correction

Since the inversion is only for the structure of D″ in the target region, other effects must be accounted for empirically. To correct for the effect of local structure near the stations and the sources, we make 'static' corrections using the time shift which gives the best correlation coefficient between the synthetic and observed seismograms. The procedure is as follows: we auto-pick the arrival on the synthetic seismogram and measure the time from the arrival time to the first peak, defining this as $T_{\pi/4}$. We then take the time window from $4T_{\pi/4}$ before the arrival time to $T_{\pi/4}$ after the arrival time, and cross-correlate the data and the synthetic. The lag time that produces the best cross-correlation is chosen as the time shift. This method is similar to differential travel time analysis, which removes the effects of source- and receiver- structure using the approximation that the S and ScS phases have the same ray paths except for the target region. The above method cannot be used when both the S phases as well as ScS phases sample D″, because that would amount to double-counting. In such cases, we use the averaged time shift for that event as the source correction and the average of the deviation from the average time shift for that station as the receiver correction, using only data for which S does not sample D″ to compute these averages. The sum of these two terms is used as the time shift for records for which S samples D″.

4. Inversion results

The initial model is PREM [*Dziewonski and Anderson,* 1981]. The source parameters (moment tensors and centroids) are fixed to the Harvard CMT solution. The S-wave velocities at points 200 km above the CMB and higher are fixed to PREM, while those

within 200 km of the CMB are the unknown parameters. We have not attempted to invert for the depth of D″, as that would require the use of shorter period waveform data. We conduct two types of inversion: (1) damped least squares inversion, (2) inversions using the eigenvectors corresponding to the n largest eigenvalues of the singular value decomposition (SVD) of the matrix of partial derivatives (Fig. 2a,b) as the basis functions for the perturbation to the starting model yielding models SVD2 and SVD3 for $n = 2$ and $n = 3$ respectively. Similar models are obtained using both of the above methods (Fig. 3).

Table 2 shows variance data. Defining the variance of the data to be 100%, the variance of the residuals (data − PREM synthetics) is 75.0%. A further variance reduction (to 72.8%) is achieved by making the time shift corrections. The residuals for the three models obtained by the inversions (DAMP, SVD2, and SVD3) are 65.0%, 65.9%, and 64.2% respectively. As all three models produce roughly the same variance reduction, the differences between these three models can be regarded as giving a rough indication of the uncertainty of the inversion results. Since the velocities at points 200 km above the CMB and higher are fixed to the initial model, the residual error is, at least in part, due to the differences between the real Earth and the Earth model (including Q) outside the study region, and also to source effects. Fig. 2d shows that while the variance computed using the Born approximation decreases monotonically as increases, the real variance computed with respect to each final model without using any approximations increases for the $n = 4$ model (SVD4) due to the non-linearity of the inversion. This further confirms the appropriateness of using the SVD3 model.

All three models in Fig. 3 show a strong velocity increase relative to PREM in the upper part of D″, but drop back to PREM in roughly the 100 km immediately above the CMB. The fact that, as shown in Fig. 3, both SVD2 and SVD3 show the same pattern, as does DAMP, supports the case that this is real rather than an artifact. To further examine this question, we conduct resolution tests (Fig. 4). We use six different starting models, as shown in Fig. 4, and compute synthetics for each model for the sources and stations in our actual inversion. We then use PREM as the starting model and conduct an inversion. The two-layered perturbations (Figs. 4a and 4b) could both be satisfactorily resolved by all three inversions. The three-layered model could be resolved by SVD3, but not by DAMP. The four-layered perturbations (Figs. 4e and 4f) could not be resolved. This supports the ability of our methods and dataset to detect the absence of an S-velocity increase (over PREM) in the 100 km immediately above the CMB. We present data on the amplitude of the partial derivatives in Fig. 2c. This figure shows that the sensitivity is greatest for the zone immediately above the CMB. On the basis of the above discussion, although there remain other possible interpretations (e.g., chemical layering, temperature effect and anisotropy), we tentatively conclude that the 'double crossing' implied by the models in Fig. 3 is likely to be real.

Acknowledgments. We thank Hiroki Senshu, Kei Hirose, and Shigenori Maruyama for valuable discussions regarding geodynamics and the Earth's deep interior. We also thank John Hernlund and an anonymous reviewer for valuable comments. Data were provided by the BDSN, CNSN, and IRIS data centers. This research was partly supported

by grants from the Japanese Ministry of Education, Science and Culture (Nos. 16740249, 17037001, and 17540392). K.K. was supported by a JSPS Fellowship for Young Scientists.

References

Avants, M., T. Lay, S.A. Russell, and E.J. Garnero (2006), Shear velocity variation within the D″ region beneath the central Pacific, *J. Geophys. Res.*, *111*, B05305, doi:10.1029/2004JB003270.

Ding, X., and D.V. Helmberger (1997), Modelling D″ structure beneath Central America with broadband seismic data, *Phys. Earth Planet. Inter.*, *101,* 245–270.

Dziewonski, A.M., and D.L. Anderson (1981), Preliminary reference Earth model, *Phys. Earth Planet. Inter.*, *25,* 297–356.

Flores, C., and T. Lay (2005), The trouble with seeing double, *Geophys. Res. Lett.*, *32*, L24305, doi:10.1029/2005GL02366.

Geller, R.J., and T. Hara (1993), Two efficient algorithms for iterative linearized inversion of seismic waveform data, *Geophys. J. Int.*, *115,* 699–710.

Geller, R.J., and T. Ohminato (1994), Computation of synthetic seismograms and their partial derivatives for heterogeneous media with arbitrary natural boundary conditions using the Direct Solution Method, *Geophys. J. Int.*, *116,* 421–446.

Hernlund, J.W., C. Thomas, and P.J. Tackley (2005), A doubling of the post-perovskite phase boundary and structure of the Earth's lowermost mantle, *Nature*, *434,* 882–886.

Kawai, K., N. Takeuchi, and R.J. Geller (2006), Complete synthetic seismograms up to 2 Hz for transversely isotropic spherically symmetric media, *Geophys. J. Int.*, *164,* 411–424.

Kendall, J.M., and C. Nangini (1996), Lateral variations in D″ below the Caribbean, *Geophys. Res. Lett.*, *23*, 399-402.

Kennett, B.L.N., S. Widiyantoro, and R.D. van der Hilst (1998), Joint seismic tomography for bulk sound and shear wave speed in the Earth's mantle, *J. Geophys. Res.*, *103*, 12,469–12,493.

Lay, T., and D.V. Helmberger (1983), A lower mantle S-wave triplication and the shear velocity structure of D″, *Geophys. J. R. Astron. Soc.*, *75,* 799–838.

Lay, T., Q. Williams, E.J. Garnero, L. Kellogg, and M.E. Wysession (1998), Seismic wave anisotropy in the D″ region and its implications, in *The Core-Mantle Boundary Region, Geodyn. Ser.*, Vol. 28, edited by M. Gurnis, et al., pp. 299–318, AGU, Washington, DC.

Murakami, M., K. Hirose, K. Kawamura, N. Sata, and Y. Ohishi (2004), Post-perovskite phase transition in $MgSiO_3$, *Science*, *304,* 855–858.

Oganov, A.R., and S. Ono (2004), Theoretical and experimental evidence for a post-perovskite phase of $MgSiO_3$ in D″ layer, *Nature*, *430,* 445–448.

Panning, M., and B. Romanowicz (2004), Inferences on flow at the base of Earth's mantle based on seismic anisotropy, *Science*, *303,* 351–353.

Takeuchi, N., R.J. Geller, and P.R. Cummins (2000), Complete synthetic seismograms for 3-D heterogeneous Earth models computed using modifed DSM operators and their applicability to inversion for Earth structure, *Phys. Earth Planet. Inter.*, *119,* 25–36.

Williams, Q. (1998), The temperature contrast across D″, in *The Core-Mantle Boundary Region, Geodyn. Ser.*, Vol. 28, edited by M. Gurnis, et al., pp. 73–81, AGU, Washington, DC.

Wysession, M.E., T. Lay, J. Revenaugh, Q. Williams, E.J. Garnero, R. Jeanloz, and L.H. Kellogg (1998), Seismic wave anisotropy in the D″ region and its implications, in *The Core-Mantle Boundary Region, Geodyn. Ser.*, Vol. 28, edited by M. Gurnis, et al., pp. 273–297, AGU, Washington, DC.

Event #	Date (Y/M/D)	Latitude	Longitude	Depth	M_w
1	1993/5/24	-23.45	-66.88	231.9	7.0
2	1993/10/19	-22.12	-65.69	278.9	6.0
3	1994/1/10	-13.28	-69.27	603.6	6.9
4	1994/4/29	-28.51	-63.22	565.9	6.9
5	1994/5/10	-28.62	-63.02	603.0	6.9
6	1994/8/19	-26.72	-63.42	562.6	6.4
7	1997/1/23	-22.04	-65.92	281.6	7.1
8	1997/11/28	-13.70	-68.90	600.5	6.6
9	1999/9/15	-20.73	-67.37	217.5	6.4
10	2000/4/23	-28.41	-63.04	607.9	6.9
11	2000/5/12	-23.72	-66.85	226.6	7.2
12	2002/10/12	-8.30	-71.66	539.4	6.9
13	2003/7/27	-20.05	-65.19	350.6	6.0
14	2004/3/17	-21.24	-65.60	297.0	6.1
15	2005/3/21	-24.86	-63.47	572.4	6.8

Table 1. Earthquakes used in this study.

Model	variance (%)	$\delta\beta$ (km/s)
PREM	75.0	-
PREM with time shift	72.8	-
DAMP	65.0	0.066
SVD2	65.9	0.081
SVD3	64.2	0.080

Table 2. Variance and averaged perturbation to shear velocity in D″ ($\delta\beta$) for each model.

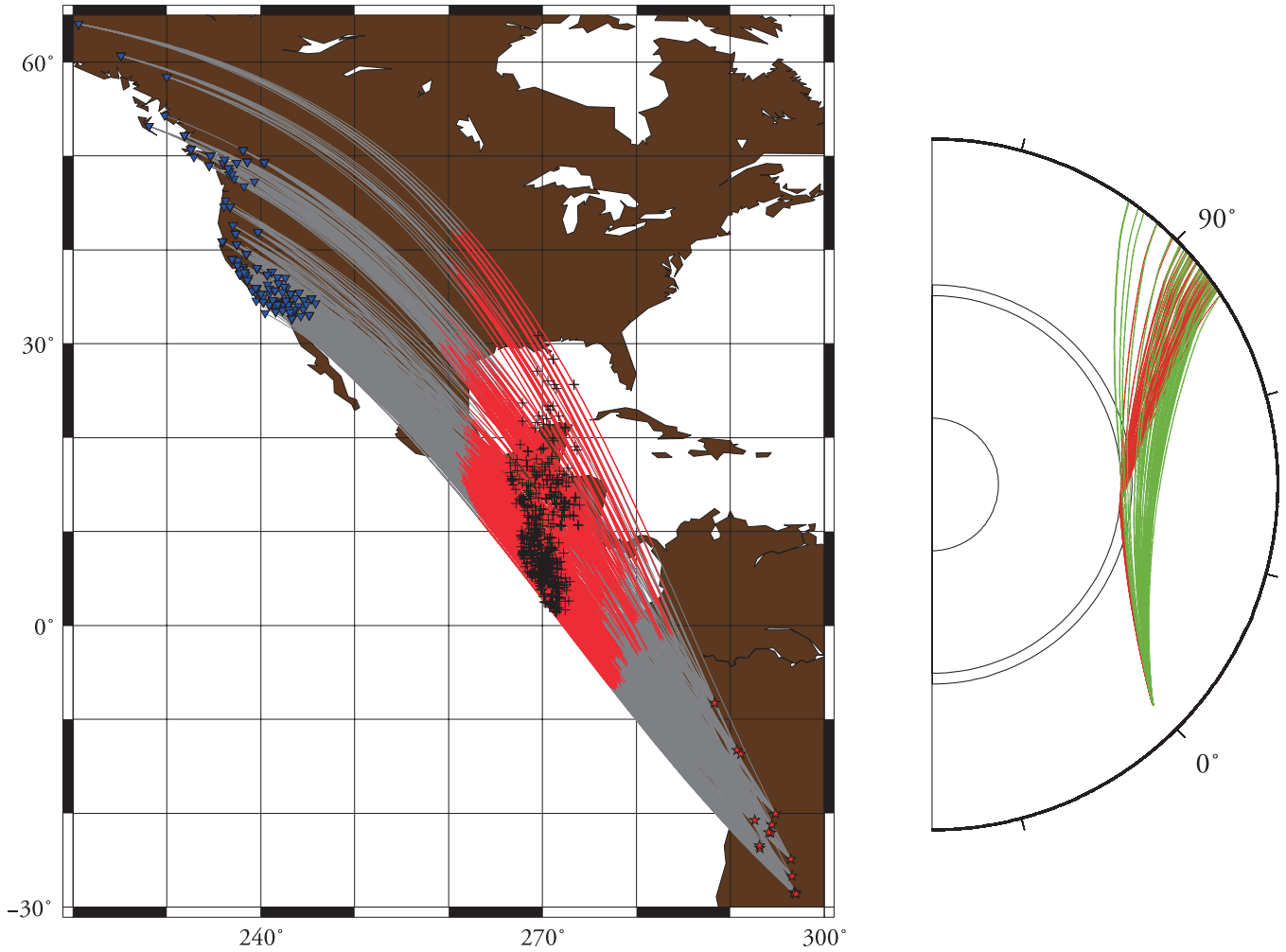

Figure 1. (Left) Event-receiver geometry, with great circle ray paths. The portions of the great circles which sample D″ are shown in red, and plus signs indicate the turning points within D″. Blue reversed triangles show the sites of North American stations (data from IRIS/USGS, SCSN, PNSN, BDSN, and CNSN) used in our study. Red stars show the fifteen intermediate and deep earthquakes studied. (Right) Cross section of rays for one event (#10) for PREM. S and ScS phases are shown in green and red, respectively.

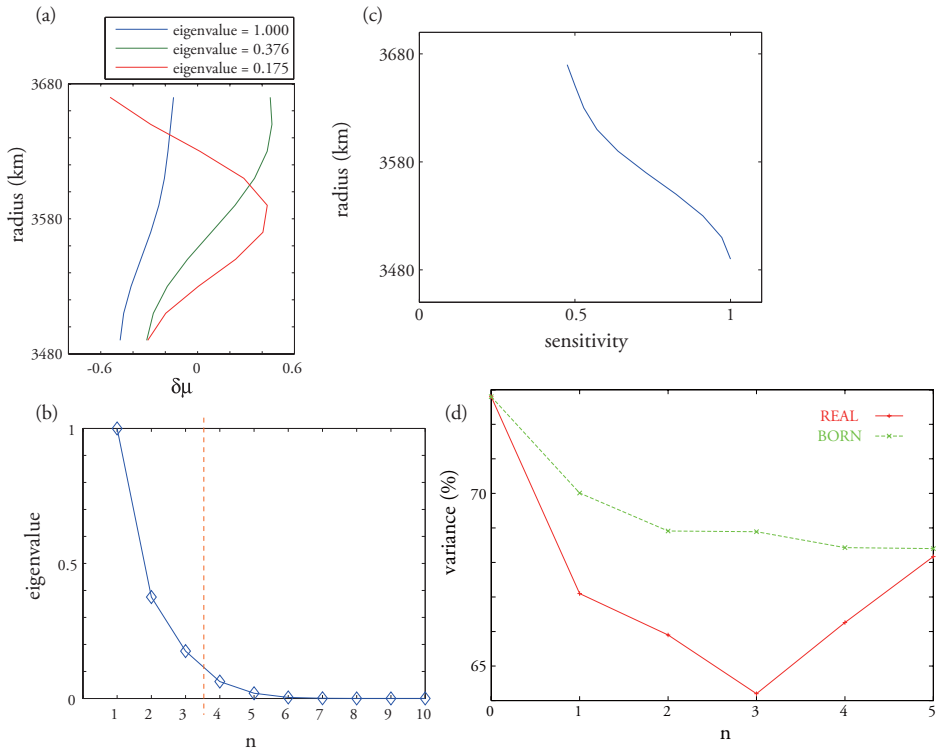

Figure 2. (a) The three eigenvectors corresponding to the three largest eigenvalues of the singular value decomposition (SVD) of the matrix of partial derivatives, which we used as the basis functions in this study. (b) The first ten eigenvalues of the SVD, with the largest eigenvalue normalized to one. (c) Sensitivity (computed from the diagonal component of the matrix of partial derivatives), normalized to a maximum value of one. (d) The actual variance reduction (computed without making any approximations) and the variance reduction computed using the Born approximation for SVD for models using the first n eigenvectors ($n = 1, 2, \cdots, 5$) as a basis.

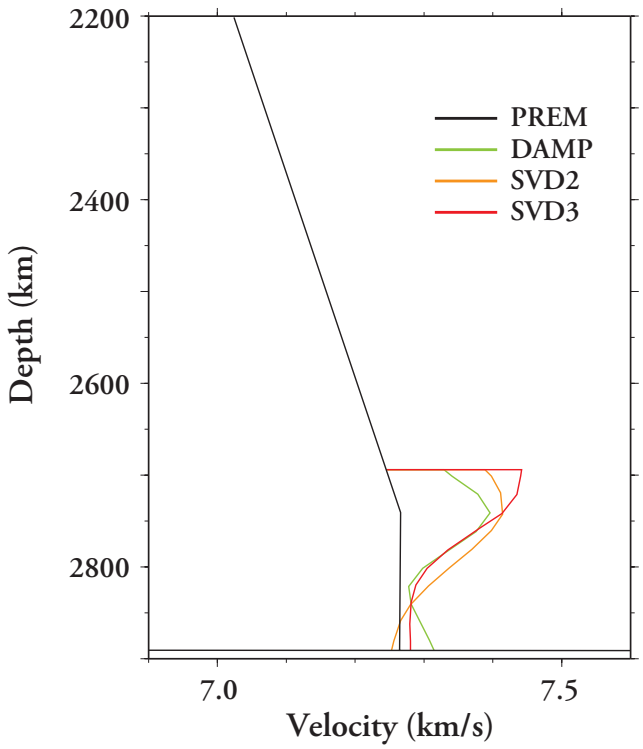

Figure 3. Results of the inversion. We obtained three basically similar S-wave velocity models: one using DAMPed least squares inversion and two using SVD inversions with two and three basis functions, yielding models SVD2 and SVD3 respectively.

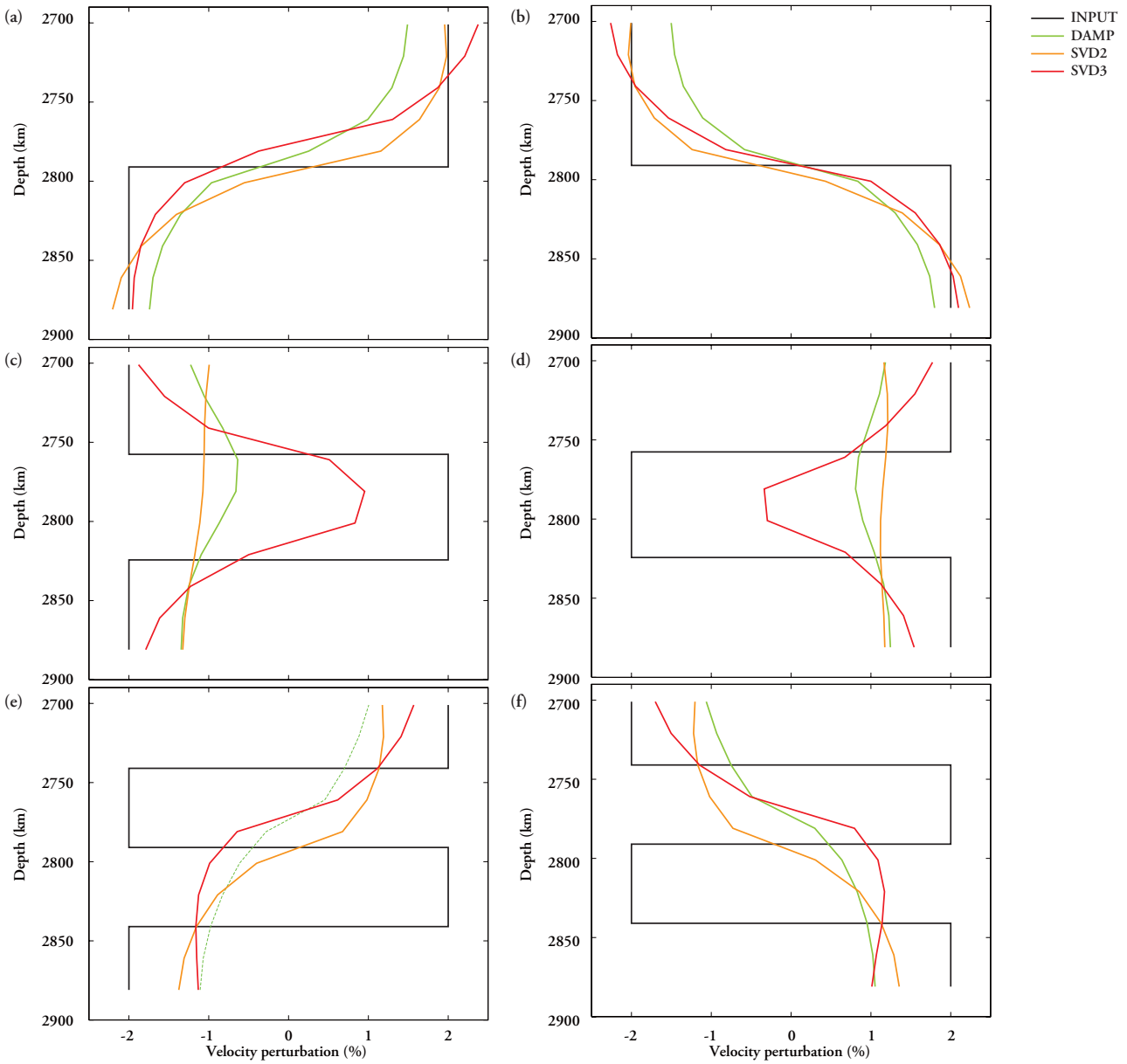

Figure 4. Resolution test for D″ structure (details in text). Our methods and present dataset can successfully resolve the two-layered models (a and b), but not the four-layered models (e and f). The details of the three-layered models (c and d) were be partially resolved by SVD3, but not by DAMP or SVD2.